Hindawi Publishing Corporation
Mathematical Problems in Engineering
Volume 2012, Article ID 865461, 11 pages
doi:10.1155/2012/865461

Research Article

Dynamic Analysis of Cracked Cantilever, Electrostatic Microactuators Using Radial Basis Functions

Ming-Hung Hsu

Department of Electrical Engineering, National Penghu University of Science and Technology, Magong, Penghu, Taiwan

Correspondence should be addressed to Ming-Hung Hsu, hsu.mh@msa.hinet.net

Received 10 July 2012; Revised 7 November 2012; Accepted 17 November 2012

Academic Editor: Slim Choura

The dynamic problems of a microactuator with a single edge crack are numerically formulated using radial basis functions. The microactuator model incorporates the taper ratio, electrode shapes, and crack length, all of which govern the dynamic behavior of microactuators. To optimize the design of a microactuator, many characteristics of various shaped cantilevers and curved electrodes are also investigated.

1. Introduction

Microelectromechanical systems exploit microscale effects to extend the range applications of actuators, accelerometers, angular rate sensors, and other devices. Elucidation of the dynamic mechanism of electrostatic microactuators contributes markedly to their design. Legtenberg et al. [1] investigated the dynamic behavior of active joints for different electrostatic actuator designs and proposed the idea of using a curved electrode to improve pull-in performance. Electrostatic actuators are widely applied in microelectromechanical systems. Electrostatic microactuator devices have a high operating frequency and low power consumption. Hong et al. [2] studied the influence of the dimensions and stress of such a device on fatigue endurance when an external force was applied to a normal microcantilever beam and a notch cantilever beam. They performed analysis simulation indicating that the stress was maximal at the fixed end. Their results showed that a deep notch in a specimen concentrate stress and thus promote specimen failure. Mehdaoui et al. [3] presented the vertical cointegration of AlSi MEMS tunable capacitors and Cu inductors in tunable LC blocks. Etxeberria and Gracia [4] proposed tunable MEMS volume capacitors for high-voltage applications. Liu et al. [5] presented actuation by electrostatic

repulsion established by nonvolatile charge injection. Gallant and Wood [6] investigated how fabrication techniques affect the performance of widely tunable micromachined capacitors. Borwick III et al. [7] analyzed a high Q microelectromechanical capacitor with large tuning range for RF filter systems. Harsh et al. [8] studied the design and realization of a flip-chip integrated microelectromechanical tunable capacitor. Osterberg et al. [9, 10] proposed a one-dimensional model and a three-dimensional model for analyzing electrostatically deformed diaphragms. Their results revealed that the electrostatic deformation calculated using the one-dimensional model is close to that obtained using a three-dimensional model. Gilbert et al. [11] analyzed the three-dimensional coupled electromechanics of microelectromechanical systems using a CoSolve-EM simulation algorithm. Elwenspoek et al. [12] studied the dynamic behavior of active joints for various electrostatic actuator designs. Shi et al. [13] presented the combination of an exterior boundary element method for analyzing electrostatics and a finite-element method for analyzing elasticity to evaluate the effect of coupling between the electrostatic force and the elastic deformation. Gretillat et al. [14] employed the three-dimensional MEMCAD and finite-element method programs to simulate the dynamics of a nonlinear actuator, taking into account squeeze-film damping. Hung and Senturia [15] developed leveraged bending and strain-stiffening methods to increase the maximum travel distance before the pull-in of electrostatic actuators. Chan et al. [16] measured the pull-in voltage and capacitance-voltage characteristic and performed two-dimensional simulations that included the electrical effects of fringing fields and finite-beam thickness to determine the material properties of electrostatic microactuators. Li and Aluru [17] developed a mixed-regime approach for combining linear and nonlinear theories to analyze large microelectromechanical structure deformations at large applied voltages. Their results demonstrated that electrostatic actuators can undergo large deformation at certain driving voltages. Chyuan et al. [18–20] established the validity and accuracy of the dual boundary element method and employed it to elucidate the effect of a variation in gap size on the levitation of a microelectromechanical comb drive. Qiao et al. [21] presented a suspension beam called a two beam to realize a parallel-plate actuator with an extended working range, but without the disadvantages of complex control circuit and high actuation voltage. In this investigation, radial basis functions are adopted to analyze how cantilever shape, damping, cracks, and electrode shape affect dynamic behavior in electrostatic actuator systems. The radial basis function scheme is applied to formulate the electrostatic field problems in matrix form. The integrity and computational accuracy of radial basis functions are demonstrated with reference to various case studies. To the author's knowledge, very few published investigates have presented a vibration analysis of a cantilever electrostatic microactuator with an edge crack using radial basis functions.

2. Radial Basis Function

A radial basis function is a real-valued function whose value depends on the distance from an origin. Kansa [22, 23] studied a given function or partial derivatives of a function with respect to a coordinate direction which is expressed as a linear weighted sum of all functional values at all mesh points along the direction that was initiated based on the concept of radial basis function. In their algorithm, the node distribution was completely unstructured. Wang and Liu [24] proposed a point interpolation meshless method that was based on radial basis functions and incorporated the Galerkin weak form for solving partial differential equations. Elfelsoufi and Azrar [25] investigated the buckling, flutter, and vibration of beams using radial basis functions. Hon et al. [26] used radial basis functions for function fitting and

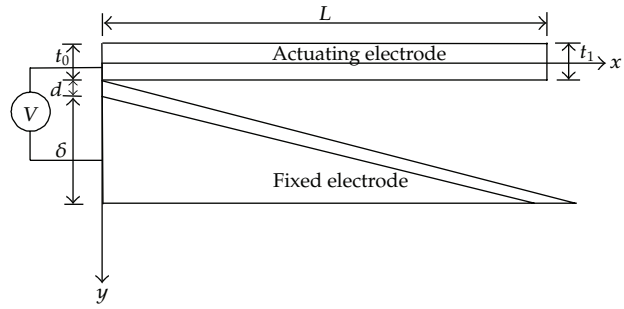

Figure 1: Schematic of a clamped-free curved electrode microactuator with an edge crack.

solving partial differential equations using global nodes and collocation procedures. Liu et al. [27] constructed shape functions with the delta function property based on radial and polynomial basis functions. In this study, shape functions are constructed using radial basis functions. A radial basis function can be expressed as follows [28, 29]:

$$B_i(x) = \sqrt{(x - x_i)^2 + c^2}, \tag{2.1}$$

where c is a constant. The radial basis function is typically used to develop the functional approximations of the following form [28, 29]:

$$v(x,t) = \sum_{i=1}^{N} a_i(t) B_i(x), \tag{2.2}$$

where a_i is the coefficient to be determined. The microcantilever deflection $v(x,t)$ denotes a sum of N radial basis functions, each associated with a different center x_i. The domain contains N collocation points. Although this nonlinear equation of the electrostatic microactuator does not have an analytical solution, numerical approaches can be adopted to solve it. These nonlinear partial differential equations are obtained numerically using the radial basis function approach, which does not require a mesh.

3. Dynamic Behavior of Clamped-Free Microactuators

Figure 1 displays the geometry of an electrostatic actuator with an edge crack close to its fixed end. Variable t_0 is the thickness of a microactuator at $x = 0$, t_1 denotes the tip thickness of a microactuator at $x = L$, and L is the length of the microbeam. An electrostatic force, introduced by the difference between the driving voltage of the curved electrode and that of the cantilever, pulls the cantilever toward the curved electrode. The electrostatic force is approximately proportional to the inverse of the square of the distance between the curved electrode and the shaped cantilever. The equation of motion of an electrostatic microactuator with an edge crack near the fixed end can be derived as [1, 30]

$$\rho A \frac{\partial^2 v}{\partial t^2} + D \frac{\partial^2}{\partial x^2}\left(EI \frac{\partial^3 v}{\partial x^2 \partial t}\right) + \frac{\partial^2}{\partial x^2}\left(EI \frac{\partial^2 v}{\partial x^2}\right) = \frac{\varepsilon_0 b \overline{V}^2 (1 + 0.65((d + S - \alpha x t_0/2L - v)/b))}{2(d + S - \alpha x t_0/2L - v)^2}, \tag{3.1}$$

where S represents the shape of the curved electrode, and is given by a polynomial such that $S = (x\delta/L)^n$, δ is the gap between the tip of a curved electrode at $x = L$ and the tip of a micro cantilever at $x = L$, α is defined as the ratio $(t_1 - t_0)/t_0$, and n is the polynomial order of the shape of the electrode. The electrode shape varies with the value of n. $\overline{V}$ is the driving voltage; E is Young's modulus of the actuator material; ε_0 is the dielectric constant of air, $\varepsilon_0 = 8.85 \times 10^{-12}$; b is the width of the microactuator; d is the initial gap, as displayed in Figure 1. The dielectric layer prevents short circuits. The cross-sectional area of a microactuator is $A(x) = bt_0(1+\alpha x/L)$, and $I(x)$ is the moment of inertia of the cross-sectional area of a microactuator and is given by $I(x) = I_0(1 + \alpha x/L)^3$ and $I_0 = bt_0^3/12$. The Kelvin-Voigt damping force $D(\partial^2/\partial x^2)(EI(\partial^3 v/\partial t \partial x^2))$ is assumed to model resistance to the actuator strain velocity. D is the Kelvin-Voigt damping coefficient. To ensure generality, Kelvin-Voigt damping effects are considered in the formulation of the equations of motion [31, 32]. Equation (3.1) depicts the fringing effects of the electrical field. The dynamic characteristics of edge-cracked beams are of considerable importance in many designs. The flexibility G caused by a crack of depth $\overline{a}$ can be determined using Broek's approximation [33] to be

$$\frac{(1-\mu^2)K_I^2}{E} = \frac{(P_b)^2}{2b}\frac{dG}{d\overline{a}}, \tag{3.2}$$

where K_I is the stress intensity factor under mode I loading; μ is Poisson's ratio; P_b denotes the bending moment at the crack; G is the flexibility of the micro cantilever. The magnitude of the stress intensity factor can be determined using Tada's formula [34], as

$$K_I = \frac{6P_b}{bt_0^2}\sqrt{\pi r t_0}F_I(r), \tag{3.3}$$

where

$$F_I(r) = \sqrt{\frac{2}{\pi r}\tan\left(\frac{\pi r}{2}\right)}\frac{0.923 + 0.199(1-\sin(\pi r/2))^4}{\cos(\pi r/2)}, \qquad r = \frac{\overline{a}}{t_0}. \tag{3.4}$$

Substituting the stress intensity factor K_I into (3.2), yields

$$G = \frac{6(1-\mu^2)t_0\int_0^r \pi r F_I^2(r)dr}{EI_0}. \tag{3.5}$$

Since

$$k_T = \frac{1}{G}, \tag{3.6}$$

the bending stiffness k_T of the cracked section of a micro cantilever can be expressed as

$$k_T = \frac{EI_0}{6(1-\mu^2)t_0\int_0^r \pi r F_I^2(r)dr}. \tag{3.7}$$

A crack can be represented as a spring of zero length and zero mass. The boundary conditions associated with (3.1) for a microactuator with an edge crack near its fixed end are given by

$$\begin{aligned} v(0,t) &= 0, \\ EI\frac{\partial^2 v(0,t)}{\partial x^2} &= k_T \frac{\partial v(0,t)}{\partial x}, \\ EI\frac{\partial v^2(L,t)}{\partial x^2} &= 0, \\ \frac{\partial}{\partial x}\left(EI\frac{\partial v^2(L,t)}{\partial x^2}\right) &= 0. \end{aligned} \tag{3.8}$$

This nonlinear equation does not have an analytical solution; however, numerical approaches can be utilized to solve it. The radial basis function approach is adopted to solve numerically these nonlinear partial differential equations. In the radial basis function approach, (2.2) is substituted into (3.1). The equation of motion of a fixed-free microbeam can be rearranged into a formula based on the radial basis function approach:

$$\begin{aligned} &\left[\frac{\partial^2 EI(x_i)}{\partial x^2}\frac{\partial^2 B_1(x_i)}{\partial x^2} \;\; \frac{\partial^2 EI(x_i)}{\partial x^2}\frac{\partial^2 B_2(x_i)}{\partial x^2} \;\; \cdots \;\; \frac{\partial^2 EI(x_i)}{\partial x^2}\frac{\partial^2 B_N(x_i)}{\partial x^2}\right]\begin{bmatrix} a_1 & a_2 & \cdots & a_N \end{bmatrix}^T \\ &\quad + \left[2\frac{\partial EI(x_i)}{\partial x}\frac{\partial^3 B_1(x_i)}{\partial x^3} \;\; 2\frac{\partial EI(x_i)}{\partial x}\frac{\partial^3 B_2(x_i)}{\partial x^3} \;\; \cdots \;\; 2\frac{\partial EI(x_i)}{\partial x}\frac{\partial^3 B_N(x_i)}{\partial x^3}\right]\begin{bmatrix} a_1 & a_2 & \cdots & a_N \end{bmatrix}^T \\ &\quad + \left[EI(x_i)\frac{\partial^4 B_1(x_i)}{\partial x^4} \;\; EI(x_i)\frac{\partial^4 B_2(x_i)}{\partial x^4} \;\; \cdots \;\; EI(x_i)\frac{\partial^4 B_N(x_i)}{\partial x^4}\right]\begin{bmatrix} a_1 & a_2 & \cdots & a_N \end{bmatrix}^T \\ &\quad + \left[D\frac{\partial^2 EI(x_i)}{\partial x^2}\frac{\partial^2 B_1(x_i)}{\partial x^2} \;\; D\frac{\partial^2 EI(x_i)}{\partial x^2}\frac{\partial^2 B_2(x_i)}{\partial x^2} \cdots D\frac{\partial^2 EI(x_i)}{\partial x^2}\frac{\partial^2 B_N(x_i)}{\partial x^2}\right]\begin{bmatrix} \frac{\partial a_1}{\partial t} & \frac{\partial a_2}{\partial t} & \cdots & \frac{\partial a_N}{\partial t} \end{bmatrix}^T \\ &\quad + \left[2D\frac{\partial EI(x_i)}{\partial x}\frac{\partial^3 B_1(x_i)}{\partial x^3} \;\; 2D\frac{\partial EI(x_i)}{\partial x}\frac{\partial^3 B_2(x_i)}{\partial x^3} \cdots 2D\frac{\partial EI(x_i)}{\partial x}\frac{\partial^3 B_N(x_i)}{\partial x^3}\right]\begin{bmatrix} \frac{\partial a_1}{\partial t} & \frac{\partial a_2}{\partial t} & \cdots & \frac{\partial a_N}{\partial t} \end{bmatrix}^T \\ &\quad + \left[DEI(x_i)\frac{\partial^4 B_1(x_i)}{\partial x^4} \;\; DEI(x_i)\frac{\partial^4 B_2(x_i)}{\partial x^4} \;\; \cdots \;\; DEI(x_i)\frac{\partial^4 B_N(x_i)}{\partial x^4}\right]\begin{bmatrix} \frac{\partial a_1}{\partial t} & \frac{\partial a_2}{\partial t} & \cdots & \frac{\partial a_N}{\partial t} \end{bmatrix}^T \\ &\quad + \left[\rho A(x_i)B_1(x_i) \;\; \rho A(x_i)B_2(x_i) \;\; \cdots \;\; \rho A(x_i)B_N(x_i)\right]\begin{bmatrix} \frac{\partial^2 a_1}{\partial t^2} & \frac{\partial^2 a_2}{\partial t^2} & \cdots & \frac{\partial^2 a_N}{\partial t^2} \end{bmatrix}^T \\ &= \left[\frac{\varepsilon_0 b\overline{V}^2\left(1+0.65\left(\left(d+S-\alpha x t_0/2L-\sum_{j=1}^{N} a_j B_j\,(x_i)\right)/b\right)\right)B_1(x_i)}{2\left(d+S-\alpha x t_0/2L-\sum_{j=1}^{N} a_j B_j(x_i)\right)^2}\right. \\ &\qquad \frac{\varepsilon_0 b\overline{V}^2\left(1+0.65\left(\left(d+S-\alpha x t_0/2L-\sum_{j=1}^{N} a_j B_j\,(x_i)\right)/b\right)\right)B_2(x_i)}{2\left(d+S-\alpha x t_0/2L-\sum_{j=1}^{N} a_j B_j(x_i)\right)^2} \\ &\qquad \left.\cdots \;\; \frac{\varepsilon_0 b\overline{V}^2\left(1+0.65\left(\left(d+S-\alpha x t_0/2L-\sum_{j=1}^{N} a_j B_j\,(x_i)\right)/b\right)\right)B_N(x_i)}{2\left(d+S-\alpha x t_0/2L-\sum_{j=1}^{N} a_j B_j(x_i)\right)^2}\right] \\ &\quad \times\begin{bmatrix} a_1 & a_2 & \cdots & a_N \end{bmatrix}^T \quad \text{for } i = 1,2,\ldots,N. \end{aligned} \tag{3.9}$$

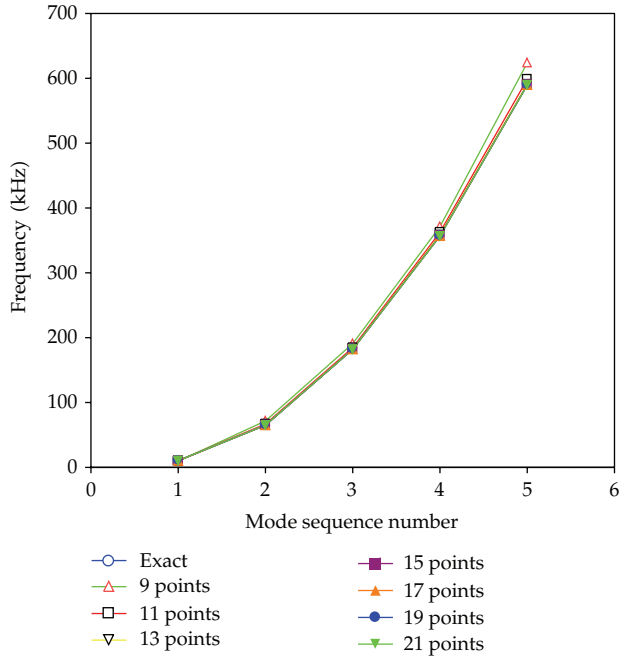

Figure 2: Frequencies of the clamped-free curved electrode microactuator obtained using radial basis function approach at various collocation points.

Based on the radial basis function approach, the boundary conditions of a clamped-free microactuator with an edge crack can be rearranged into matrix forms as

$$\begin{aligned}
&\left[B_1(x_1)\ \ B_2(x_1)\ \ \cdots\ \ B_N(x_1)\right]\left[a_1\ \ a_2\ \ \cdots\ \ a_N\right]^T = [0],\\
&\left[EI(x_1)\frac{\partial^2 B_1(x_1)}{\partial x^2}\ \ EI(x_1)\frac{\partial^2 B_2(x_1)}{\partial x^2}\ \ \cdots\ \ EI(x_1)\frac{\partial^2 B_N(x_1)}{\partial x^2}\right]\left[a_1\ \ a_2\ \ \cdots\ \ a_N\right]^T\\
&\quad = \left[k_T\frac{\partial B_1(x_1)}{\partial x}\ \ k_T\frac{\partial B_2(x_1)}{\partial x}\ \ \cdots\ \ k_T\frac{\partial B_N(x_1)}{\partial x}\right]\left[a_1\ \ a_2\ \ \cdots\ \ a_N\right]^T,\\
&\left[EI(x_N)\frac{\partial^2 B_1(x_N)}{\partial x^2}\ \ EI(x_N)\frac{\partial^2 B_2(x_N)}{\partial x^2}\ \ \cdots\ \ EI(x_N)\frac{\partial^2 B_N(x_N)}{\partial x^2}\right]\left[a_1\ \ a_2\ \ \cdots\ \ a_N\right]^T = [0],\\
&\left[EI(x_N)\frac{\partial^3 B_1(x_N)}{\partial x^3}\ \ EI(x_N)\frac{\partial^3 B_2(x_N)}{\partial x^3}\ \ \cdots\ \ EI(x_N)\frac{\partial^3 B_N(x_N)}{\partial x^3}\right]\left[a_1\ \ a_2\ \ \cdots\ \ a_N\right]^T\\
&\quad + \left[\frac{\partial EI(x_N)}{\partial x}\frac{\partial^2 B_1(x_N)}{\partial x^2}\ \ \frac{\partial EI(x_N)}{\partial x}\frac{\partial^2 B_2(x_N)}{\partial x^2}\ \ \cdots\ \ \frac{\partial EI(x_N)}{\partial x}\frac{\partial^2 B_N(x_N)}{\partial x^2}\right]\\
&\quad \times \left[a_1\ \ a_2\ \ \cdots\ \ a_N\right]^T = [0].
\end{aligned} \tag{3.10}$$

4. Numerical Results

The following figures summarize the results thus obtained. Figure 2 shows the frequencies of a clamped-free curved electrode microactuator. The material and geometric parameters of the actuator considered herein are $E = 150\,\text{GPa}$, $\delta = 30\,\mu\text{m}$, $b = 5\,\mu\text{m}$, $t_0 = 2\,\mu\text{m}$, $r = 0$,

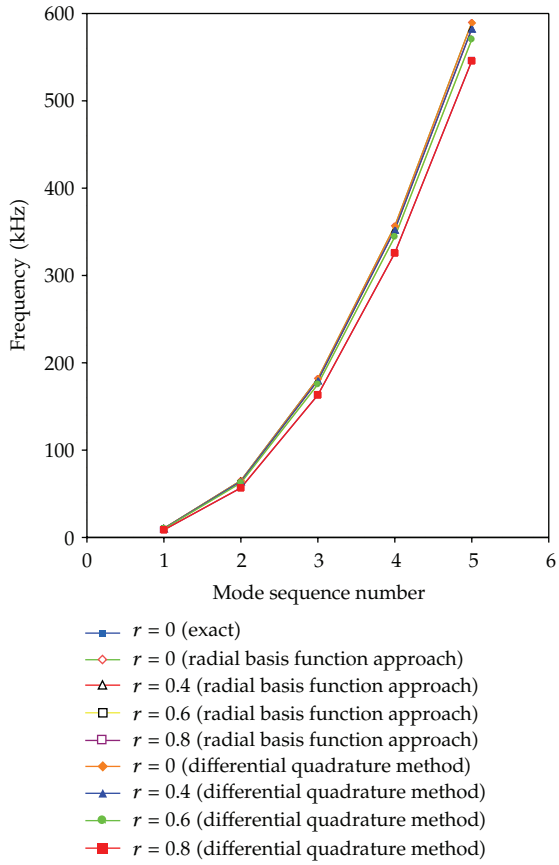

Figure 3: Frequencies of clamped-free curved electrode microactuators for various values of r.

$\alpha = 0$, and $d = 2\,\mu$m [1, 35]. The figure plots the analytical solutions and the numerical results obtained using radial basis function approach. Numerical results indicate that the estimated frequencies remain stable even when only fifteen collocation points are considered. They also suggest that the frequencies calculated using the radial basis function approach are extremely close to the exact solutions. Figure 3 shows the frequencies of a clamped-free curved electrode microactuator for various crack depths. The frequency falls, as the crack depth increases. The crack depth significantly affects the frequencies of the micro cantilever. Computational results solved using radial basis function approach are compared with numerical results obtained using the differential quadrature method. Figure 4 compares the tip deflections of an actuating electrode for various driving voltages and electrode shapes. Changing the electrode shape in an electrostatic microactuator is an effective technique for varying the electrostatic force distribution therein. Numerical and measured results suggest that the tip deflections calculated using the radial basis function approach are in good agreement with published experimental results [1]. Numerical results demonstrate that the pull-in voltage declines gradually, as the value of n increases. Figure 5 plots the tip responses of the microactuator with different α values. The tip deflections of the micro cantilever drop, as α increases. As α increases, the applied voltage required to cause a particular deflection of the tip of the micro cantilever increases. The cantilever shapes substantially influence the pull-in behavior

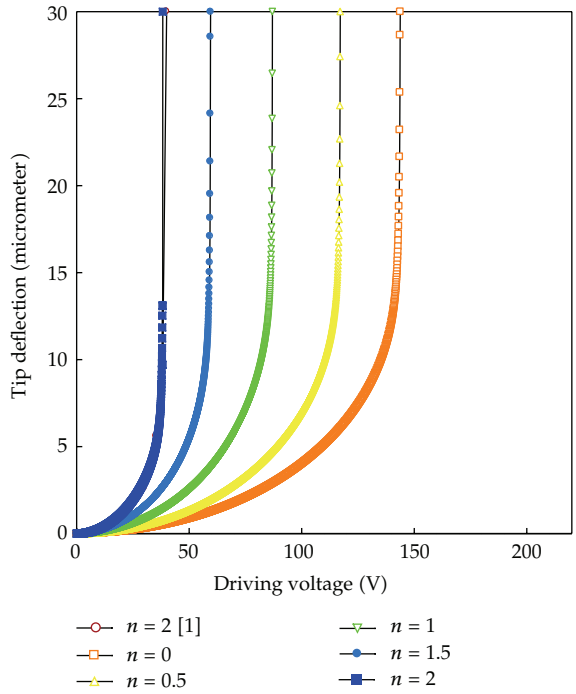

Figure 4: Comparison of tip deflections of variously shaped actuating electrodes.

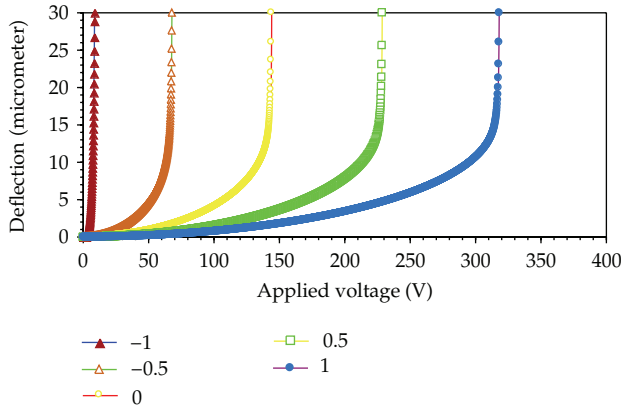

Figure 5: Tip responses of microactuators for different values of α.

of microactuators. Figure 6 plots the tip responses of the microactuator for various values of r. Notably, the tip deflection increases with crack depth. The depth of the crack significantly affects the tip response. Figure 7 shows the variation of the tip responses of the actuator with D. Because of recent advances in stably responding and high performance actuator structures, the enhancement of damping has become a very significant issue. The numerical results in this example show that internal damping can significantly affect the dynamic behavior of the actuator system. Strong residual vibration occurs in a system with a zero internal damping coefficient.

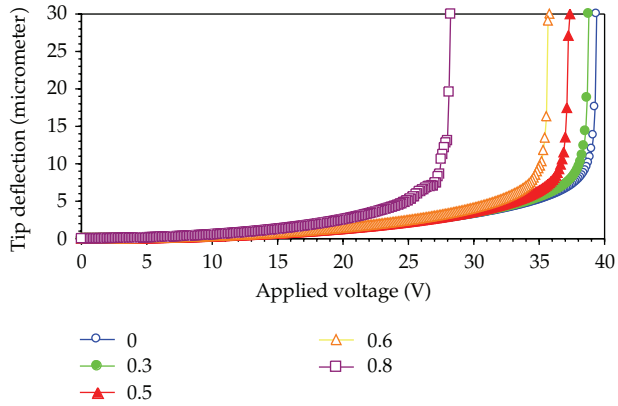

Figure 6: Tip responses of microactuators for various values of r.

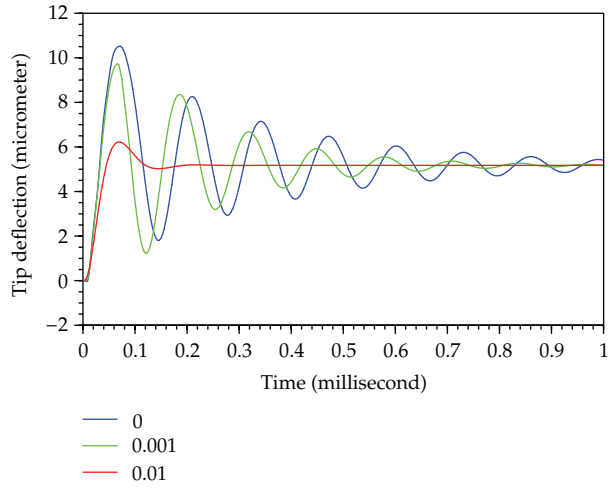

Figure 7: Tip responses of microactuators for various values of D.

5. Conclusions

This work examines the radial basis functions for dynamic problems of an electrostatic actuator with a crack. The effects of internal damping, electrode shape, edge cracking, and cantilever shape on the pull-in behavior of electrostatic microstructures are investigated. The frequency of the microcantilever declines, as the crack depth increases. The value of radial basis functions that describe the pull-in behavior of a microactuator with an edge crack is determined.

References

[1] R. Legtenberg, J. Gilbert, S. D. Senturia, and M. Elwenspoek, "Electrostatic curved electrode actuators," *Journal of Microelectromechanical Systems*, vol. 6, no. 3, pp. 257–265, 1997.

[2] H. Hong, J. N. Hung, and Y. H. Guu, "Various fatigue testing of polycrystalline silicon microcantilever beam in bending," *Japanese Journal of Applied Physics*, vol. 47, no. 6, pp. 5256–5261, 2008.

[3] A. Mehdaoui, M. B. Pisani, R. Fritschi, P. Ancey, and A. M. Ionescu, "Vertical co-integration of AlSi MEMS tunable capacitors and Cu inductors for tunable LC blocks," *Microelectronic Engineering*, vol. 84, no. 5–8, pp. 1369–1373, 2007.
[4] J. A. Etxeberria and F. J. Gracia, "Tunable MEMS volume capacitors for high voltage applications," *Microelectronic Engineering*, vol. 84, no. 5–8, pp. 1393–1397, 2007.
[5] Z. Liu, M. Kim, N. Y. M. Shen, and E. C. Kan, "Actuation by electrostatic repulsion by nonvolatile charge injection," *Sensors and Actuators A*, vol. 119, no. 1, pp. 236–244, 2005.
[6] A. J. Gallant and D. Wood, "The role of fabrication techniques on the performance of widely tunable micromachined capacitors," *Sensors and Actuators A*, vol. 110, no. 1–3, pp. 423–431, 2004.
[7] R. L. Borwick III, P. A. Stupar, J. DeNatale et al., "A high Q, large tuning range MEMS capacitor for RF filter systems," *Sensors and Actuators A*, vol. 103, no. 1-2, pp. 33–41, 2003.
[8] K. F. Harsh, B. Su, W. Zhang, V. M. Bright, and Y. C. Lee, "Realization and design considerations of a flip-chip integrated MEMS tunable capacitor," *Sensors and Actuators A*, vol. 80, no. 2, pp. 108–118, 2000.
[9] P. Osterberg, H. Yie, X. Cai, J. White, and S. Senturia, "Self-consistent simulation and modeling of electrostatically deformed diaphragms," *Proceedings of the IEEE Micro Electro Mechanical Systems*, pp. 28–32, 1994.
[10] P. M. Osterberg and S. D. Senturia, "M-test: a test chip for MEMS material property measurement using electrostatically actuated test structures," *Journal of Microelectromechanical Systems*, vol. 6, no. 2, pp. 107–118, 1997.
[11] J. R. Gilbert, R. Legtenberg, and S. D. Senturia, "3D coupled electro-mechanics for MEMS: applications of CoSolve-EM," in *Proceedings of the IEEE Micro Electro Mechanical Systems Conference*, pp. 122–127, February 1995.
[12] M. Elwenspoek, M. Weustink, and R. Legtenberg, "Static and dynamic properties of active joints," in *Proceedings of the 8th International Conference on Solid-State Sensors and Actuators and Eurosensors*, pp. 412–415, June 1995.
[13] F. Shi, P. Ramesh, and S. Mukherjee, "Simulation methods for micro-electro-mechanical structures (MEMS) with application to a microtweezer," *Computers and Structures*, vol. 56, no. 5, pp. 769–783, 1995.
[14] M. A. Gretillat, Y. J. Yang, E. S. Hung et al., "Nonlinear electromechanical behavior of an electrostatic microrelay," in *Proceedings of the International Conference on Solid-State Sensors and Actuators*, pp. 1141–1144, June 1997.
[15] E. S. Hung and S. D. Senturia, "Extending the travel range of analog-tuned electrostatic actuators," *Journal of Microelectromechanical Systems*, vol. 8, no. 4, pp. 497–505, 1999.
[16] E. K. Chan, K. Garikipati, and R. W. Dutton, "Characterization of contact electromechanics through capacitance-voltage measurements and simulations," *Journal of Microelectromechanical Systems*, vol. 8, no. 2, pp. 208–217, 1999.
[17] G. Li and N. R. Aluru, "Linear, nonlinear and mixed-regime analysis of electrostatic MEMS," *Sensors and Actuators A*, vol. 90, no. 3, pp. 278–291, 2001.
[18] S. W. Chyuan, Y. S. Liao, and J. T. Chen, "An efficient method for solving electrostatic problems," *Computing in Science and Engineering*, vol. 5, no. 3, pp. 52–58, 2003.
[19] S. W. Chyuan, Y. S. Liao, and J. T. Chen, "Computational study of variations in gap size for the electrostatic levitating force of MEMS device using dual BEM," *Microelectronics Journal*, vol. 35, no. 9, pp. 739–748, 2004.
[20] Y. S. Liao, S. W. Chyuan, and J. T. Chen, "Efficaciously modeling the exterior electrostatic problems with singularity for electron devices," *Circuits and Devices Magazine*, vol. 20, no. 5, pp. 25–34, 2004.
[21] D. Y. Qiao, W. Z. Yuan, and X. Y. Li, "A two-beam method for extending the working range of electrostatic parallel-plate micro-actuators," *Journal of Electrostatics*, vol. 65, no. 4, pp. 256–262, 2007.
[22] E. J. Kansa, "Multiquadrics—a scattered data approximation scheme with applications to computational fluid-dynamics-I surface approximations and partial derivative estimates," *Computers and Mathematics with Applications*, vol. 19, no. 8-9, pp. 127–145, 1990.
[23] E. J. Kansa, "Multiquadrics—a scattered data approximation scheme with applications to computational fluid-dynamics-II solutions to parabolic, hyperbolic and elliptic partial differential equations," *Computers and Mathematics with Applications*, vol. 19, no. 8-9, pp. 147–161, 1990.
[24] J. G. Wang and G. R. Liu, "A point interpolation meshless method based on radial basis functions," *International Journal for Numerical Methods in Engineering*, vol. 54, no. 11, pp. 1623–1648, 2002.
[25] Z. Elfelsoufi and L. Azrar, "Buckling, flutter and vibration analyses of beams by integral equation formulations," *Computers and Structures*, vol. 83, no. 31-32, pp. 2632–2649, 2005.

[26] Y. C. Hon, M. W. Lu, W. M. Xue, and Y. M. Zhu, "Multiquadric method for the numerical solution of a biphasic mixture model," *Applied Mathematics and Computation*, vol. 88, no. 2-3, pp. 153–175, 1997.
[27] G. R. Liu, X. Zhao, K. Y. Dai, Z. H. Zhong, G. Y. Li, and X. Han, "Static and free vibration analysis of laminated composite plates using the conforming radial point interpolation method," *Composites Science and Technology*, vol. 68, no. 2, pp. 354–366, 2008.
[28] G. B. Wright, *Radial basis function interpolation: numerical and analytical developments [Ph.D. thesis]*, University of Colorado at Boulder, 2003.
[29] M. D. Buhmann, *Radial Basis Functions: Theory and Implementations*, Cambridge University Press, New York, NY, USA, 2003.
[30] K. S. Chen and K. S. Ou, "Development and verification of 2D dynamic electromechanical coupling solver for micro-electrostatic-actuator applications," *Sensors and Actuators A*, vol. 136, no. 1, pp. 403–411, 2007.
[31] R. W. Clough and J. Penzien, *Dynamics of Structures*, McGraw-Hill, New York, NY, USA, 1975.
[32] S. S. Rao, *Mechanical Vibrations*, Addison-Wesley, New York, NY, USA, 1990.
[33] D. Broek, *Elementary Engineering Fracture Mechanics*, Martinus Nijhoff, Leiden, The Netherlands, 1986.
[34] H. Tada, P. C. Paris, and G. R. Irwin, *The Stress Analysis of Crack Handbook*, Professional Engineering, 2000.
[35] Y. Liu, K. M. Liew, Y. C. Hon, and X. Zhang, "Numerical simulation and analysis of an electroactuated beam using a radial basis function," *Smart Materials and Structures*, vol. 14, no. 6, pp. 1163–1171, 2005.